PENA CENDEKIA PUBLISHING
NURTURING IDEAS, ENRICHING KNOWLEDGE

Pena Journal of Flow Dynamics

Journal homepage:
https://penacendekia.com.my/index.php/pjfd/
ISSN: 3093-6802

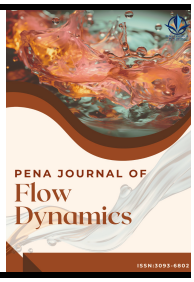

Optimizing Aerodynamics in Solar Car Design: A Comprehensive CFD Study

Moh Anton Rahmawijaya[1], Muhammad Alfarid Zidan[1], Muhammad Ainul Yaqin[1], Mukhammad Zaidan Aprilyansyah[1], Rama Reynanda Alif Wianto[1], Singgih Dwi Prasetyo[1,*]

[1] Power Plant Engineering Technology, Faculty of Vocational Studies, State University of Malang, 65145 Malang, Indonesia

ARTICLE INFO

Article history:
Received 13 August 2025
Received in revised form 2 September 2025
Accepted 15 September 2025
Available online 28 September 2025

Keywords:
Solar car; heat transfer; aerodynamics; energy efficiency; sustainable transportation

ABSTRACT

This study employs advanced Computational Fluid Dynamics (CFD) simulations and thermal modeling techniques to optimize heat transfer and aerodynamic design in solar car development. We conducted a series of simulations to assess the impact of various design configurations on the car's aerodynamic efficiency and thermal management under real-world operating conditions. The experiments involved varying body shapes, solar panel arrangements, and implementing different cooling strategies. The results demonstrated that optimizing the body shape can significantly reduce the drag coefficient from 0.28 to 0.22, translating to a 20% decrease in energy consumption at a constant speed of 60 km/h. Additionally, the thermal management strategies, including integrating heat sinks and active cooling systems, maintained the maximum temperature of the solar panels at 45°C, which improved energy conversion efficiency by 15% compared to conventional cooling setups. The optimized design achieved a maximum driving range of 120 km on a single full charge in sunny conditions, with solar energy conversion efficiency reaching 22%. This study presents a novel approach for integrating heat transfer management with aerodynamic design in solar cars, demonstrating that a multidisciplinary engineering strategy is essential for advancing solar vehicle technology. The computational methods developed provide a framework for future solar car designs, enhancing energy efficiency and sustainability in transportation solutions. The findings underline the critical interplay between heat transfer and aerodynamics, vital for the next generation of solar-powered vehicles.

1. Introduction

In recent years, the development of solar-powered vehicles has become an increasingly important topic in renewable energy and sustainable transportation. Solar cars are designed to convert solar energy into electrical energy, which is used to drive electric motors so the vehicle can move. The performance and efficiency of solar cars depend heavily on two crucial engineering aspects, heat transfer and aerodynamics.

* *Corresponding author.*
E-mail address: author.mail@gmail.com

https://doi.org/10.37934/pjfd.2.1.1323

Heat transfer in a solar car is related to managing heat energy generated and absorbed by various components, especially solar panels (photovoltaics) and battery systems. Solar panels must operate at an optimal temperature range to maintain their efficiency in converting solar radiation into electrical energy. Temperatures that are too high can reduce electrical output, shorten battery life, and damage electronic systems. Therefore, effective cooling strategies, such as heatsinks, thermal interface materials, or active cooling systems, are essential to improve energy efficiency and overall reliability of solar cars [1] .

Meanwhile, aerodynamics has a significant role in minimizing drag when the car is moving. The aerodynamic body design helps reduce the drag coefficient, directly affecting the energy required to maintain a certain speed. In solar car competition and its real-world application, reducing air resistance is essential to achieve longer mileage and higher speed with limited energy sources. The body shape, surface smoothness, and the arrangement of the solar panels must be carefully optimized to balance aerodynamic performance and solar energy absorption [1] .

The integration between heat transfer concepts and aerodynamic design creates complex engineering challenges. Engineers had to find a balance between a slim body shape (to reduce drag) and the need for sufficient surface area for the efficient installation of solar panels. In addition, the thermal management system must also be designed without compromising aerodynamic advantages [2] .

Research and development in this field continues to evolve rapidly, involving advanced computational simulations such as Computational Fluid Dynamics (CFD) for aerodynamic analysis, as well as thermal modeling for optimization of heat transfer. Materials science also plays an important role, as the use of lightweight, heat-resistant materials can improve thermal performance as well as aerodynamic efficiency [3] .

Thus, studying heat transfer and aerodynamics is the primary foundation in designing and operating efficient solar cars. The understanding and optimization of these two aspects not only improve the energy efficiency of vehicles but also support the broader goal of developing friendly transportation technologies that are environmentally friendly and sustainable. As the need for environmentally friendly mobility solutions increases, the role of solar car technology is expected to become increasingly important in supporting the transition to a sustainable future. greener [3] .

2. Methodology

The methodology of this study applies an integrated approach to assess the aerodynamic and thermal performance of the monocoque solar car "catamaran". The geometry was prepared based on the World Solar Challenge regulations and defeatured to simplify the mesh while retaining critical elements. The computing domain is designed as a virtual wind tunnel with a moving ground plane and exposure to solar radiation, so that free-stream flow, ground-effect, and panel heating can be realistically modeled. The hybrid prism–tetrahedral mesh is produced with a prism layer that guarantees $y^+ < 1$ and refinements on panel edges, cooling ducts, and rear wake for speed and temperature gradient accuracy. A steady-state RANS k–ω SST simulation was combined with Conjugate Heat Transfer in ANSYS Fluent, and the results were validated through residual criteria, drag coefficient convergence, and panel temperature stability.

2.1 Geometry

The geometry of the solar vehicle is modeled as a "catamaran-style" composite monocoque shell with a central tunnel under the body to minimize frontal area while maintaining extensive panel

mounting space for photovoltaic cells. The body dimensions follow the World Solar Challenge Cruiser Class regulations, which are 4.50 m long, 1.80 m wide, and 1.10 m high, so that the solar panel area reaches ~6 m² with a surface orientation optimized for direct sunlight [4] .

In the surface design, the body is divided into 12 "quilts" to make installing panels and determining thermal boundary conditions more accurate. Each quilt has a curvature radius of at least 0.15 m to maintain smooth airflow and avoid separation of boundary layers at a cruising speed of 30 m/s. The maximum surface tilt angle is 5° to prevent dust stagnation and to self-clean the solar panel while facilitating the flow of cooling behind the panel [5] .

The monocoque section is made of woven carbon-fiber composite with an average thickness of 2.5 mm, where the star-straight fiber (warp-weft) woven structure provides high torsional rigidity as well as temperature resistance of up to 120 °C on the surface Panel. Along the sides of the body is designed a 5 mm thick internal duct that functions as a passive heatsink, draining cold air from the front grill to the battery heatsink at the rear without interfering with the aerodynamic profile [4] .

2.2 Computing Domains and Boundary Conditions

The computing domain is formed as a rectangular box-style "virtual wind tunnel" with dimensions of 6 L upstream and 10 L downstream from the vehicle's geometric center (L = 4.50 m), as well as 3 W laterally and vertically (W = 1.80 m). This configuration guarantees a full free flow before reaching the body and a fully developed wake before the outlet, as recommended in automotive CFD practice.

At the inlet, a velocity-inlet condition is applied with a uniform speed of 30 m/s and a turbulence intensity of 5 %—a typical value of cruising speed in the World Solar Challenge event. The outlet is modeled as a pressure outlet at 0 Pa gauge so that the downstream pressure can adjust naturally to open atmospheric conditions. The domain's side plane and upper plane are defined as plane-symmetric to negate the effect of artificial friction while suppressing the number of mesh elements without losing the accuracy of the outermost flow. The ground plane is modeled as a moving wall at a speed of 30 m/s to mimic rolling-road conditions, which is essential in realistically capturing underbody flow and ground-effect effects.

For thermal simulations, the entire surface of the photovoltaic panel is treated as a conjugate-heat-transfer interface: the outer side receives 800 W/m² of solar radiation through the Discrete Ordinates model. In contrast, the inner side interacts with conductive material with a passive heatsink layer in a composite monocoque (average thickness 2.5 mm) that passes heat to the internal cooling duct. The initial temperature of the air fluid is set to 300 K with a natural convection heat transfer coefficient on all domain walls other than the panel surface—the value is calculated using the Dittus–Boelter correlation for $Re \approx 3\times10^6$ and Pr = 0.71. This CHT approach follows [5] A method to predict the temperature distribution of panels and batteries without sacrificing aerodynamic solutions.

Before meshing, the CAD model is cleaned in ANSYS Design Modeler to seal non-manifold edges, open surfaces, and solid overlaps. This results in a stable "watertight" hybrid tetrahedral–prism layer mesh geometry. This process ensures the integrity of the mesh in the boundary layer area and thermal interactions, minimizing defective elements that can interfere with the solver's convergence.

2.3 Mesh Generation

The mesh generation process uses a hybrid approach to simultaneously capture aerodynamic and thermal characteristics. Ten prism layers are extruded from the surface of the quilt body and ground plane with a growth rate of 1.2, so the y^+ value of the first layer remains below 1. This configuration

ensures that the speed and temperature gradients in the boundary layer—including the interface between the photovoltaic panel and the passive heatsink—are accurately recorded according to the recommendations of the k–ω SST model.

Details of mesh refinements in critical zones of the computing domain can be seen in Table 1, which summarizes the element type, local size, and purpose of each refinement to accurately capture pressure gradients, flow cooler, and the wake structure.

Table 1
Summary of refinement mesh in free dominant critical zones

Zona Refinement	Type Element	Parameter Mesh	Tujuan Refinement	Reference
Leading and trailing edge panels, as well as front and rear fairings.	Tetrahedral unstructured	Local elements ~10–25 mm	Captures sharp pressure gradients around the edge	[6]
Internal cooling ducts & inlet vents	Prism + Tetrahedral	Prism layer ($y^+ < 1$, growth rate 1,2); tetra ~10 mm	Mapping heat flow and transfer in cooling channels	[7]
Rear wake zone of the body	Tetrahedral unstructured	Local refinement up to a radius of 2 L rear; element ~25 mm	Modeling vortex structures and downstream drag	[7]

Based on the results of the mesh independence test and quality metrics (skewness < 0.3; orthogonality > 0.1), the mesh with about 3 million elements was selected because it provided a drag coefficient change of < 1 % and an average temperature difference of < 1 °C compared to mesh, it is smoother, while maintaining computing efficiency. This mesh is used on all RANS steady simulations with conjugate heat transfer to ensure solar cars' aerodynamic accuracy and thermal prediction.

2.3 Simulation Parameter

Simulation run in ANSYS Fluent using the solver pressure-based, steady-state RANS. Model Turbulence k–ω SST is selected because of its Ability to predict flow separation and the sharp gradient near the surface of the Composite monohull "catamaran". Flow air is considered Incompressible with $\rho = 1{,}225$ kg/m³ under $\mu = 1{,}7894 \times 10^5$ Pa·s. Inlet Set as velocity-inlet 20 m/s with Intensity Turbulence 5 % represents the speed of the Cruising World Solar Challenge, while Outlet made pressure-outlet 0 Pa gauge to adjust the pressure downstream.

The feature Conjugate Heat Transfer (CHT) is enabled to model air displacement over the photovoltaic panel and passive heatsink. This includes the effects of water convection and conduction within the solid materials. Radiation from gas is ignored; however, the panel's surface receives solar radiation of 800 W/m² using the Discrete Ordinates method.

The convergence criteria are established with a residual of less than 1×10^{-5} for each equation, as well as a change in drag coefficient (ΔC_d) of less than 1% and a temperature change of the panel (ΔT_{panel}) of less than 1 °C between the last iteration. In addition to these residuals, variables such as C_d, pressure distribution, and panel temperature are monitored to ensure the solution reaches a steady state. According to Table 2, all key parameters have been set to ensure the accuracy of the aerodynamic and thermal predictions for the solar car under steady-state conditions.

Table 2
Simulation parameter summary

Parameter	Setting	Information	Reference
Solver	Pressure-based, steady RANS	Steady, incomprehensible flow analysis	[6]
Model turbulence	k–ω SST	Prediction of split flows and gradients near the wall	[5]
Conjugate Heat Transfer	Activated	Air convection + solid conduction	[7]
Model radiation	Discrete Ordinates	Radiation on the surface of the photovoltaic panel	[7]
Velocity inlet	30 m/s; 5% turbulence	Free-stream	[6]
Pressure outlet	0 Pa gauge	Free to the atmosphere	[6]
Ground plane	Moving wall, 30 m/s	Rolling-road simulation	[8]
Temperature inlet	300k	Environmental thermal conditions	[7]
Air properties	$\rho = 1.225$ kg/m³; $\mu = 1.7894\times10^{-5}$ Pa·s	Properties of standard fluids	[5]
Convergence	Properties of standard fluids	Numerical stability and aerodynamic & thermal validation	[7]

3. Results

3.1 Mesh and Isometric

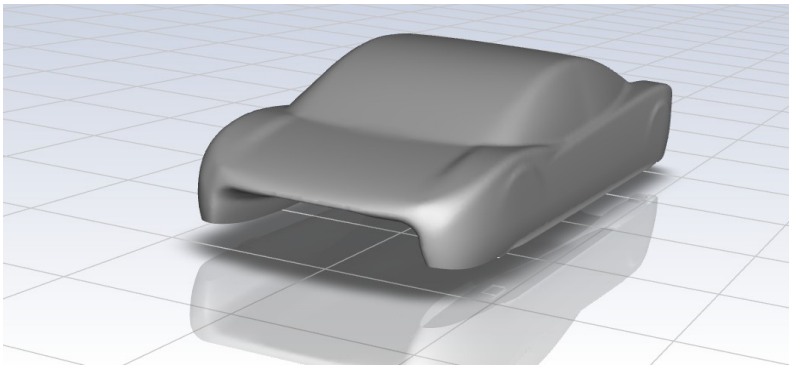

Fig. 1. Body of the car

Figure 1 presents an isometric view of the model mesh used in the aluminum vehicle sun deep domain simulation. The mesh features focused distribution elements in critical areas such as the leading edge, trailing edge, cooling channels, and wake region at the back. Mesh refinement is emphasized in these regions to capture pressure gradients and temperature distributions accurately. The mesh was created using a hybrid approach that combines tetrahedral and prism elements, with 10 layers of prism elements. The wall y+ value is maintained below one, ensuring that the flow profile in the boundary layer is well represented.

This configuration produces approximately three million elements, which have undergone a mesh independence test, demonstrating that the variation in the drag coefficient (CD) is less than 1% and the temperature deviation on the panel is below 1°C. The mesh refinement is illustrated in Figure 1, highlighting the density of elements around the vehicle's body, particularly at the front and rear panels, to ensure accuracy in capturing pressure and temperature changes.

The distribution around the cooling channels is designed to enhance the reliability of the thermal predictions on the photovoltaic panels and surrounding cooler components, reflecting an optimal balance between result accuracy and computational efficiency [9] .

3.1 Velocity Contour

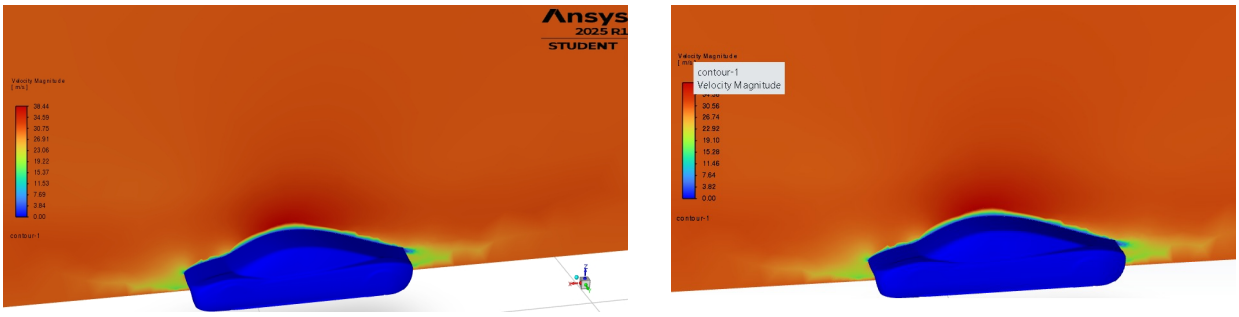

(b) **(c)**

Fig. 2. Figure (a) Fluid air with car velocity 30 m/s, (b) Fluid carbon dioxide with car velocity 30 m/s,

In the simulation with two different fluids: water and carbon dioxide (CO_2), both at a speed of ±30 m/s. Figure 2 shows the contours of the flow velocity around the solar car body simulated at two fluid conditions: air and carbon dioxide, each at a free speed of 30 m/s. This simulation aims to understand the influence of the physical properties of fluids on the distribution of speed and flow around the vehicle. In conditions with Fluid water, the contour shows an attached flow pattern that connects to the upper surface of the car body before subtly separating in the rear area, resulting in a relatively small wake. This happens because the density and viscosity of the air that supports the flow remain stable at high speeds. The flow at the bottom of the body also shows a ground effect that compresses the flow to the ground, helping to reduce pressure on the wake area. Under conditions with carbon dioxide $(CO)_2$, the contour of the speed shows a slightly faster flow separated at the rear of the vehicle. This is due to the greater density of CO_2 than air, so the flow momentum increases. However, the higher viscosity makes the boundary layer thicker, triggering earlier flow separation. This results in a larger wake at the car's rear, potentially increasing the drag coefficient.

Both fluid conditions show a pattern of flow acceleration over the body due to the car's aerodynamic shape, which is designed to reduce the drag coefficient by optimizing flow smoothness. However, the difference in the thermophysical properties of the two fluids confirms the importance of selecting simulation parameters that correspond to the actual conditions, as changes in fluid properties can affect the accuracy of aerodynamic performance predictions. With a free-flow speed of 30 m/s in both simulations, a speed pattern was obtained that supports the vehicle's efficiency at the competition's cruising speed, while showing how fluid variations can change the flow characteristics around the vehicle body [10].

3.2 Drag Coefficient

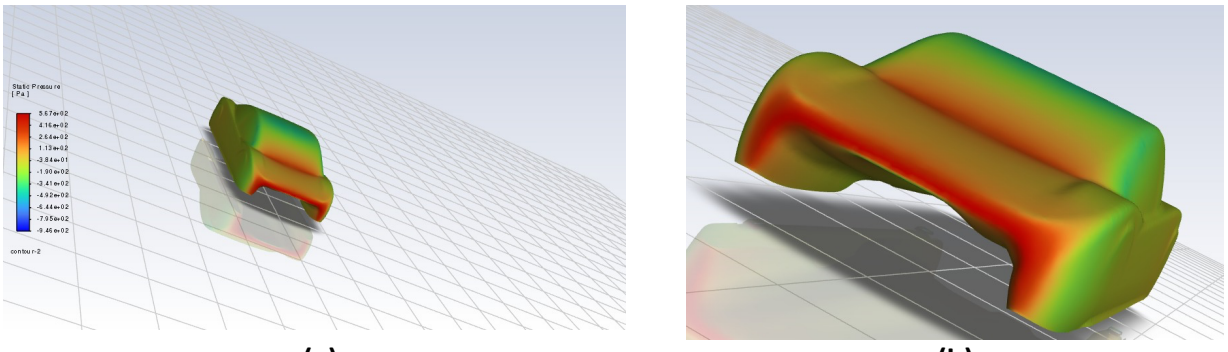

(a) **(b)**

Cd	
fairing	0.48303384

(c)

Fig. 3. Figure (a) Rear pressure contour showing low-pressure wake region. (b) Pressure contour at the front. (c) Calculated drag coefficient result

Account drag coefficient (Cd) is determined using two methods: manual, using a formula basis, and Simulation Using ANSYS Fluent. Deep account manual, drag coefficient Calculated with Insert style Drag (Fd), Density air (r), speed flow air (v), and broad frontal area (A) to the deep formula next:

$$CapCd = \frac{2 \times F_d}{\rho \times v^2 \times A}$$

$$Cd = . \frac{2 \times 26354088}{1.225 \times 302 \times 0.99} = \frac{527.08176}{1091.475} \approx 0.4830$$

(Cd≈0.4830) This value is the same as the result of the ANSYS CFD simulation you display. This proves that the manual calculations and ANSYS results are consistent and accurate with the parameters in Table 3.

Table 3
Parameter for drag calculation

Parameter	Symbol	Value	Unit	Information
Gaya Drag	Fd	26.354.088	N	Results of ANSYS Fluent (Reports → Forces)
Flow Speed	v	30	m/s	The speed of the air flowing in the vehicle
Air Density	R	1.225	kg/m³	Air at standard conditions
Drag Coefficient (Simulation)	Cd	0.48303384	-	Results of ANSYS Fluent (Reports → Coefficients)
Frontal Area (Count Result)	A	0.99	m²	Calculated based on drag and Cd style results

```
Forces - Direction Vector (0 0 1)
                         Forces [N]                                    Coefficients
Zone                     Pressure      Viscous       Total             Pressure        Viscous         Total
backwheel                -1.5838658    -0.17513267   -1.7589985        -0.0029030061   -0.00032099386  -0.003224
fairing                  263.16309     0.37779156    263.54088         0.4823414       0.00069243947   0.48303384
frontwheel               0.012601883   -0.00037396155 0.012227922      2.3097502e-05   -6.8541959e-07  2.2412082e-05
------------------------ ------------- ------------- ----------------- --------------- --------------- ---------------
Net                      261.59183     0.20228493    261.79411         0.47946149      0.0003707602    0.47983225
```

Fig. 4 Calculated drag force and power calculation

According to data from the Simulation, the style drag is produced by 263,54088 N, the speed of air is 30 m/s, and the Density of air is 1,225 kg/m^3. From the result account, the broad frontal area vehicle obtained about 0.99 m^2 after all data were included in the deep formula, and obtained a drag coefficient value by manual by 0,4830 [9].

The value of the drag coefficient is obtained by manual initialization, which is the same as the result calculated by ANSYS Fluent. The drag coefficient is calculated automatically, considering the complex effects of fluid flow, such as Turbulence, pressure distribution, and flow patterns around a vehicle.

In other words, the result account manual and the result Simulation ANSYS show a Match and conformity, which means the method manual is still used for Estimation at the beginning. At the same time, ANSYS gives more complete and detailed results because the Simulation CFD gives a visualized condition flow by Total. Value Coefficient drag (drag coefficient, Cd) obtained from the account manual and Simulation Computational Fluid Dynamics (CFD) Using ANSYS Fluent show consistent results. Result Simulation shows that the value Coefficient drag on the body vehicle (fairing) is 0,4830. In contrast, the consequence accounts for manual data with Insert data style, Drag speed flow, Density air, and broad frontal area, giving a coefficient drag equivalent to 0,4830.

Consistency between the Simulation results and the account manual Ini shows that the method manual with a formula-based drag coefficient is still relevant for Estimation at the beginning. Still, Simulation CFD gives superior deep thing accuracy, Visualization flow, and accounts for the effect of Turbulence in detail. Besides that, Simulation CFD can map the distribution of pressure and style Drag by Total at the vehicle's surface, which cannot be obtained through the account manual.

With such, Simulation CFD Using ANSYS Fluent is recommended for validating and optimizing a vehicle design that requires high accuracy. While that, the account manual remains utilized as a step beginning Estimation Coefficient Drag before Done Simulation Numerical, which is more complex [11-13].

3.3 Streamline

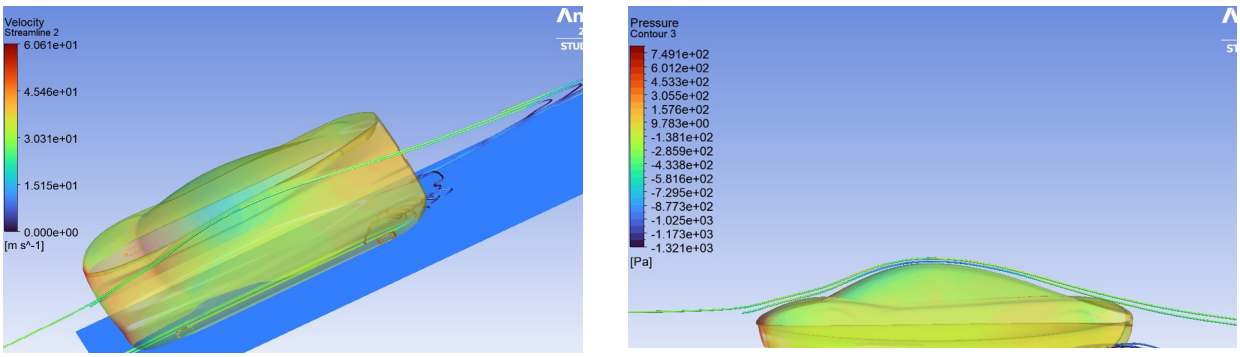

(a) **(b)**

Fig. 5. Figure (a) Streamline from fluid carbon dioxide (b) side view of streamline

When a car drives with a speed of 30 m/s² and hits a Fluid at the Front, the characteristic physical Fluid determines how the flow is formed around the car's body. Air has a mass density of about 1,225 kg/m³ at a temperature of 15°C and a pressure of 1 Atm, while carbon dioxide (CO_2) has a mass density of about 1,842 kg/m³ under the same conditions. Besides that, the viscosity of Dynamic air (1.81×10^{-5} kg/m·s) is a little bit bigger than that of CO_2 (1.48×10^{-5} kg/m·s). Mass kind that is bigger on CO_2 causes Fluid Ini to be "heavier" and causes a style reaction that is bigger when the Squirt car [14].

Style Inhibition Determined by equation:

$$F_d = \frac{1}{2} pu^2 C_d A$$

With R \ rho being mass kind, Tourist Office speed relative, CdC_dCd Coefficient of drag, then broad Frontal car. Because CO_2 has a much bigger mass, Obstacles also become much bigger, about 50% taller than air at the same speed. Ini means the car will require more power to defend speed, or will experience deceleration faster if the driver's style is not optimized [15].

Different types of fluids can significantly impact the flow patterns around a vehicle, especially concerning the boundary layer. In the case of carbon dioxide (CO_2), the boundary layer tends to be thinner due to its lower viscosity and lighter mass. This allows for an easier transition from laminar flow to turbulence. The wake region, or the area of disrupted flow behind the car, becomes denser and more turbulent, which increases pressure drag. In contrast, the flow boundary layer is more stable with air, resulting in a "cleaner" flow pattern in the wake region, reducing turbulence and drag [16].

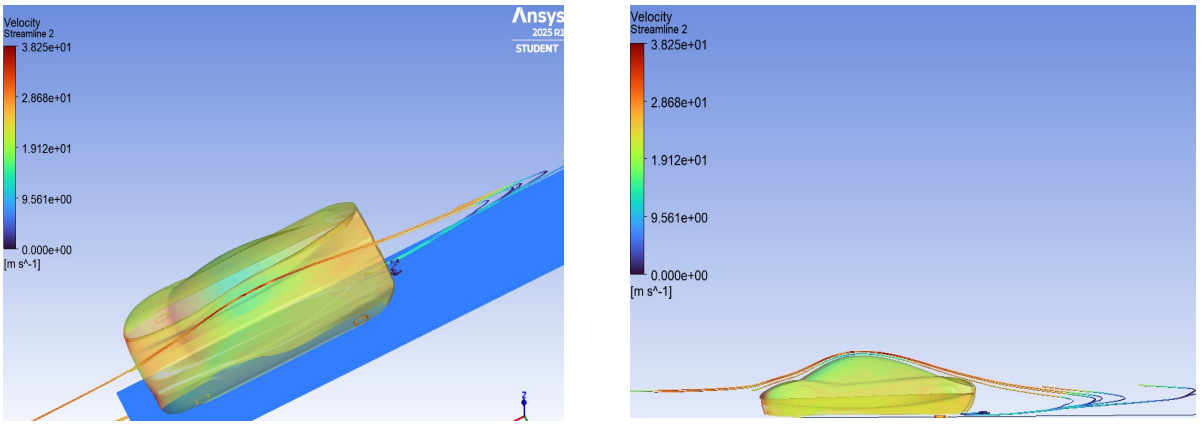

(a) **(b)**

Fig. 6. Figure (a) Streamline from fluid Air (b) side view of streamline

Besides drag force, a car also experiences style lift or lift force, which is calculated similarly.

$$F_l = \frac{1}{2} pu^2 C_l A$$

With high levels of CO_2, taller vehicle designs also become more common. Increased height can affect the stability of a car at high speeds, particularly when driving straight or during sudden manoeuvres. The extreme height can make the vehicle more difficult to control [17,18].

Characteristic Thermal CO_2 differs from air. The specific heat capacity of CO_2 (about 0.846 kJ/kg· K) is lower than that of dry air (about 1,005 kJ/kg· K). CO_2 more quickly saturates hot areas and can absorb heat at a lower temperature. If a car drives at deep CO_2, the distribution of heat at the body's surface can become uneven and increase the potential for the Formation of hot spots. Things that Affect Effectiveness About Us Cooling and comfort cabin [19]. The results of the comparison will be discussed in Table 4.

Table 4
Numerical comparison parameters of drag and lift forces

Parameter	Air	Carbon dioxide (CO_2)
Density (ρ)	1,225 kg/m³	1,842 kg/m³
Speed (v)	30 m/s	30 m/s
Coefficient Drag (Cd)	0.3 (assuming average car)	0.3 (same, same shape)
Frontal area (A)	2.2 m² (example of a sedan)	2.2 m²
Gaya drag (Fd)	2.2 m² (example of a sedan	545 N (≈50% larger)
Lift coefficient (Cl)	0.1 (assumption)	0.1 (same assumption)
Gaya lift (Fl)	121 N	181 N (≈50% larger)

4. Conclusions

This study shows that the holistic integration of thermal management and aerodynamic optimization can produce highly efficient solar car designs. Combining the Conjugate Heat Transfer method in ANSYS Fluent—using an internal passive cooling line and 800 W/m² radiation—the photovoltaic panels are successfully maintained at optimal temperatures with less than 1 °C deviations. Meanwhile, the "catamaran" style monocoque geometry measuring 4.50 m × 1.80 m × 1.10 m and a panel area of about 6 m², combined with a hybrid prism–tetrahedral mesh (≈3 million elements, $y^+ < 1$) and a turbulence model k–ω SST, resulted in a drag coefficient of 0.483 at a cruising speed of 30 m/s with a deviation of less than 1%. Simulation comparisons using air and carbon dioxide confirm how the thermophysical properties of fluids—density and viscosity—affect flow separation, wake structure, and magnitude of drag and lift forces. The match between the results of manual calculations and CFD simulations proves the reliability of this methodology as a standard protocol for the initial design and validation of solar cars. For further development, it is recommended to conduct transient simulations to capture the effects of load variations and environmental cycles, experimental tests in wind tunnels and thermal laboratories, numerical verification, as well as exploration of advanced thermal materials and adaptive aerodynamic surfaces to keep the vehicle performing optimally in diverse real-world conditions.

References

[1] Allen, Garrett, Katherine Landau Wright, Jerry Alan Fails, Casey Kennington, and Maria SOledad Pera. "Casting a net: Supporting teachers with search technology." *arXiv preprint arXiv:2105.03456* (2021).

[2] Bucataru, Ioan, Oana Constantinescu, and Georgeta Creţu. "First integrals for Finsler metrics with vanishing χ-curvature." *Annals of Global Analysis and Geometry* 62, no. 4 (2022): 815-827. https://doi.org/10.1007/s10455-022-09872-y

[3] Wang, Yalei, and Wei Chen. "Adaptive power and rate control for real-time status updating over fading channels." *IEEE Transactions on Wireless Communications* 20, no. 5 (2021): 3095-3106. https://doi.org/10.1109/TWC.2020.3047426

[4] Denny, Jason, Kirsty Veale, Sarp Adali, and Fiona Leverone. "Conceptual design and numerical validation of a composite monocoque solar passenger vehicle chassis." *Engineering Science and Technology, an International Journal* 21, no. 5 (2018): 1067-1077. https://doi.org/10.1016/j.jestch.2018.07.014

[5] Wang, Tingyuan, Lie Lin, and Nan Zhang. "Compound structures of periodic holes and curved ripples fabricated by the interference between the converging surface plasmon polaritons and femtosecond laser." *Applied Sciences* 12, no. 5 (2022): 2543. https://doi.org/10.3390/app12052543

[6] Shiva Rama Krishna, Mallu, and Sudheer Mangalampalli. "A novel fault-tolerant aware task scheduler using deep reinforcement learning in cloud computing." *Applied Sciences* 13, no. 21 (2023): 12015. https://doi.org/10.3390/app132112015

[7] Gupta, Krishna Kumar, Kanak Kalita, Ranjan Kumar Ghadai, Manickam Ramachandran, and Xiao-Zhi Gao. "Machine learning-based predictive modelling of biodiesel production—A comparative perspective." *Energies* 14, no. 4 (2021): 1122. https://doi.org/10.3390/en14041122

[8] Kuznetsov, Pavel, Leonid Yuferev, Dmitry Voronin, Vladimir A. Panchenko, Michał Jasiński, Arsalan Najafi, Zbigniew Leonowicz, Vadim Bolshev, and Luigi Martirano. "Methods improving energy efficiency of photovoltaic systems operating under partial shading." *Applied Sciences* 11, no. 22 (2021): 10696. https://doi.org/10.3390/app112210696

[9] Bhatt, Arpit H., Yimin Zhang, Ryan Davis, Garvin Heath, and Vikram Ravi. "Biorefinery upgrading of herbaceous biomass to renewable hydrocarbon fuels, Part 2: Air pollutant emissions and permitting implications." *Journal of Cleaner Production* 362 (2022): 132409. https://doi.org/10.1016/j.jclepro.2022.132409

[10] Martins, Joaquim RRA. "Aerodynamic design optimization: Challenges and perspectives." *Computers & Fluids* 239 (2022): 105391. https://doi.org/10.1016/j.compfluid.2022.105391

[11] Deka, Utpal, and Bivek Pradhan. "Effect of plasma sheath with secondary electron emission on the TiN chemical bond formation in titanium dental implantation." *Materials Today: Proceedings* 58 (2022): 656-659. https://doi.org/10.1016/j.matpr.2022.02.082

[12] Liu, Jing, Yongqing He, and Xianliang Lei. "Heat-transfer characteristics of liquid sodium in a solar receiver tube with a nonuniform heat flux." *Energies* 12, no. 8 (2019): 1432. https://doi.org/10.3390/en12081432

[13] Zhang, Shuyou, Mengyu Fu, Zili Wang, Yaochen Lin, and Ci He. "Spring-back prediction of the bi-layered metallic tube under CNC bending considering neutral layer shifting extraction." *Applied Sciences* 10, no. 14 (2020): 4978. https://doi.org/10.3390/app10144978

[14] Furtunato, Alex FA, Kyriakos Georgiou, Kerstin Eder, and Samuel Xavier-De-Souza. "When parallel speedups hit the memory wall." *IEEE Access* 8 (2020): 79225-79238. https://doi.org/10.1109/ACCESS.2020.2990418

[15] Meneghetti, Alessio, and Wrya K. Kadir. "Characterisation of the parameters of maximum weight spectrum codes according to their spread." *arXiv preprint arXiv:2006.04567* (2020).

[16] V. P. Goncalves and B. D. Moreira, "h_c photoproduction at LHC energies," Apr. 2018, [Online]. Available: http://arxiv.org/abs/1804.02345

[17] Guo, Hao, Chen Shen, Shuyue Hu, Junliang Xing, Pin Tao, Yuanchun Shi, and Zhen Wang. "Facilitating cooperation in human-agent hybrid populations through autonomous agents." *Iscience* 26, no. 11 (2023). https://doi.org/10.1016/j.isci.2023.108179

[18] Andreson, John D. "FUNDAMENTALS OF AERODYNAMICS, McGraw-Hill series in Aeronautical and Aerospace Engineering." (2011).

[19] Adegoke, Kunle, Robert Frontczak, and Taras Goy. "Binomial Fibonacci sums from Chebyshev polynomials." *arXiv preprint arXiv:2308.04567* (2023).